Scaling coefficient for three-dimensional grain coalescence of ZnO on Si(111)

Marcel Ruth and Cedrik Meier
Experimental Physics, University of Paderborn, 33098 Paderborn, Germany
(Received 18 April 2012; revised manuscript received 18 October 2012; published 11 December 2012)

Grain-rotation-induced coalescence is a well-known growth mechanism of granular/polycrystalline systems in two dimensions. In three-dimensional (3D) crystals there are more degrees of freedom, and influences of the substrate play an important role. In the present work we analyze the 3D coalescence of ZnO grains on Si(111) by thermal annealing under O_2 atmosphere. Atomic force microscopy and electron backscatter diffraction measurements reveal a significant increase in the mean grain diameter and a reorientation that matches the substrate orientation. This structural reorganization leads to a substantial enhancement of the electronic layer quality. We describe the grain growth with a diffusive model and find a volume scaling coefficient of 1.5. This proves that the additional degrees of freedom significantly accelerate grain-rotation induced coalescence in three dimensions.

DOI: 10.1103/PhysRevB.86.224108 PACS number(s): 68.35.−p, 68.55.−a, 81.40.Ef

Thin-film deposition is one of the key technologies in the fabrication of semiconductor devices. Besides electronic contacts and insulating barriers like high-k dielectrics, the growth of semiconductor films itself must be well controlled. Understanding the formation of poly- and monocrystalline thin films is thus essential for the development of new deposition processes. ZnO, a versatile material for electronic, optoelectronic, and photonic devices in the UV spectral range, has already been grown on many different substrates.[1,2] Besides heteroepitaxy on sapphire (Al_2O_3), silicon carbide (SiC), and gallium nitride (GaN) and homoepitaxy[3,4] on hydrothermally grown ZnO substrates, several groups have reported successful growth of ZnO(0001) on a Si(111) surface and potential buffer-layer materials to overcome the large misfit[5] and different thermal expansion coefficients.[6] Consequently, Si is an interesting candidate as substrate material due to the abundance of silicon wafers of outstanding quality and the highly developed planar Si technology. As ZnO is difficult to structure by dry or wet etching, overgrowth of ZnO on patterned Si templates could open novel ways for ZnO nanostructures.

Different thermal expansion coefficients often limit the growth temperatures in heteroepitaxy. Together with a large lattice mismatch this leads to polycrystalline layers with small grains. Such layers often do not exhibit optical and electronic properties of monocrystalline films and have to be treated *ex situ*.

Several authors have used statistical models to describe coalescence and growth in granular films.[7–12] Moldovan *et al.*[13] have suggested a grain-rotation-induced coalescence process and described its formation kinetics using statistical physics. Experimental evidence for this process has been given by Moore *et al.*[14] by direct observation of coalescence in colloidal crystals. It should be noted, however, that both works are limited to two dimensions.

In this work, we give experimental evidence for grain-rotation-induced coalescence in three dimensions in the highly relevant ZnO(0001)/Si(111) system, which has not been demonstrated experimentally so far. However, sublattice-specific ordering of epitaxial ZnO films was studied by Redondo-Cubero and coworkers.[15]

Photoluminescence (PL) measurements show the change in the optical and electronical properties. High-resolution x-ray diffraction (HRXRD), atomic force microscopy (AFM), scanning electron microscopy (SEM), and electron backscatter diffraction (EBSD) measurements prove the grain coalescence and reorientation.

All samples presented in this work are grown in a vertical molecular beam epitaxy system. Zinc (Zn) is thermally evaporated using a double-zone effusion cell. Oxygen radicals (O) are supplied via a radio-frequency plasma source ($\nu = 13.56$ MHz, $P = 300$ W). During growth, the oxygen background pressure is in the range of 10^{-5} Torr. The Si(111) substrates are cleaned in acetone and isopropanol. Then the surface oxide is removed chemically in buffered oxide etch so that a hydrogen-passivated surface is created. Before growth, the hydrogen capping is removed at 650 °C for 15 min inside the vacuum. Then the substrate temperature is reduced to the growth temperature of 150 °C. To prevent substrate oxidation we deposit one monolayer of Zn before the ignition of the oxygen plasma. Then we grow a 200-nm-thick ZnO film under stoichiometric conditions. To control the recrystallization and coalescence of the ZnO film, the sample is stepwise exposed to temperatures from 350° up to 1050 °C *ex situ* under an oxygen (O_2) atmosphere.

Mean grain sizes are investigated as a function of the annealing temperature. As the determination of particle sizes in nanocrystalline materials is nontrivial, different methods have their advantages and disadvantages. While XRD obviously probes the bulk of the sample volume, its drawbacks are that the particle size distribution cannot be directly determined and the instrument resolution poses an upper limit for the measurable particle diameter. AFM is a powerful tool to measure the morphology of the surface. Here, we use AFM to obtain the particle size distribution and the mean grain diameters. We validate this approach by comparison with XRD data and cross-section SEM images of a subset of the samples. The latter techniques allow us to gain insight also to the bulk of the sample.

AFM measurements were performed in a commercial setup using a silicon cantilever with a tip radius of <7 nm in dynamic mode. For determination of the grain diameter, we

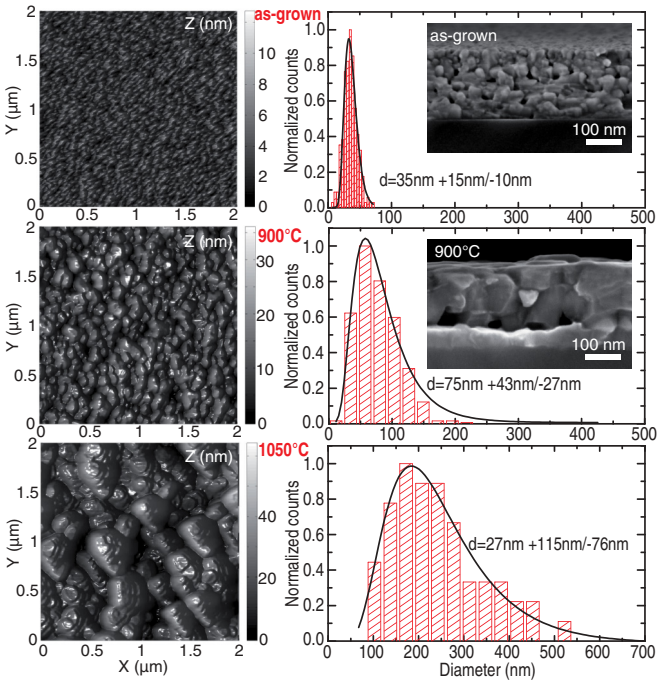

FIG. 1. (Color online) Determination of the mean grain size by histograms (right) obtained via AFM measurements (left) for as-grown samples and samples annealed at 900° and at 1050 °C. Insets: Cross-section SEM pictures of the cleaved edges.

have manually determined histograms by metering each single grain in enlarged AFM images. The resulting histograms were fitted with a log-normal distribution as suggested, e.g., by Granqvist and Buhrman.[10] Figure 1 shows the histograms and fits for the as-grown sample and for samples annealed at 900° and 1050 °C. Two different AFM scan settings were used, according to the different grain sizes. For annealing temperatures below 800 °C, a field size of 0.5 × 0.5 μm and a pixel size of 256 × 256 were used (pixel-pixel distance ∼2 nm). At temperatures of 900 °C and above, the field size was increased to 2 × 2 μm, leading to a pixel-pixel distance of around 8 nm. As the mean grain diameters obtained are around 32 nm at lower temperatures and up to 240 nm at higher temperatures, for small grains, errors are dominated by the tip radius of the AFM.

These surface grain diameters were then verified to be equivalent to the grain sizes in the bulk of the samples by three methods.

(i) Cross-section SEM images, shown as insets in Fig. 1, were taken. The cleaved edges of the different samples clearly exhibit grain sizes in the entire ZnO layer that are consistent with the AFM measurements. However, it should be noted that the grains are somewhat anisotropic in size, which might contribute to the width of the size distribution.

(ii) EBSD measurements of the sample annealed at 1050 °C were used to visualize the grain orientations and to obtain a grain size histogram (shown in the Supplemental Material).[16] The EBSD size distribution was fitted with a log-normal distribution as well. From this fit a mean grain diameter of $d = (244 + 129/-69)$ nm was obtained, which is in good agreement with the diameter obtained from the AFM data, $d = (227 + 115/-76)$ nm.

(iii) As AFM tip convolution effects are most critical for the smallest particle sizes, we performed an $\omega - 2\theta$ XRD measurement for the as-grown sample and obtained the grain size from Scherrer's equation. The full width at half-maximum (FWHM) for the ZnO(0002) reflex is $\beta = 0.2976° = 0.0052$ rad, denoting a particle diameter for the ZnO of $d_{\mathrm{as-grown,XRD}} = 27.9$ nm. This result agrees fairly well with the mean grain diameter determined by AFM of $d_{\mathrm{as-grown,AFM}} = 35$ nm, taking into account that the Scherrer formula delivers only a lower bound to the crystallite size due to the fact that other factors contribute to the width of the diffraction peak as well. From the instrument-limited XRD line width of the reference Si(111) reflex, we can also obtain an upper limit for the largest reasonably determinable grain diameter. From this reflex, we obtain from Scherrer's equation $d_{\mathrm{Si,XRD}} = 621$ nm — clearly smaller than the 1-cm single-crystalline substrate. Thus, keeping in mind that the largest grain diameters are in the range of several 100 nm, AFM is the best method for this application, as it delivers reliable results for all grain sizes under consideration.[16]

The determined mean grain diameters are plotted against the annealing temperature in Fig. 2 [(blue) diamonds]. The associated asymmetric errors of the mean grain diameter have been calculated from the grain distributions containing 68% of the grains using the corresponding dispersion coefficient.[16] In the low-temperature regime, below 800 °C, there is no significant change in the size of the grains. At higher temperatures, the diameter increases up to a value of 237 nm at 1000 °C and 227 nm at 1050 °C. As the fitting of the diameter at 1000 °C is somewhat

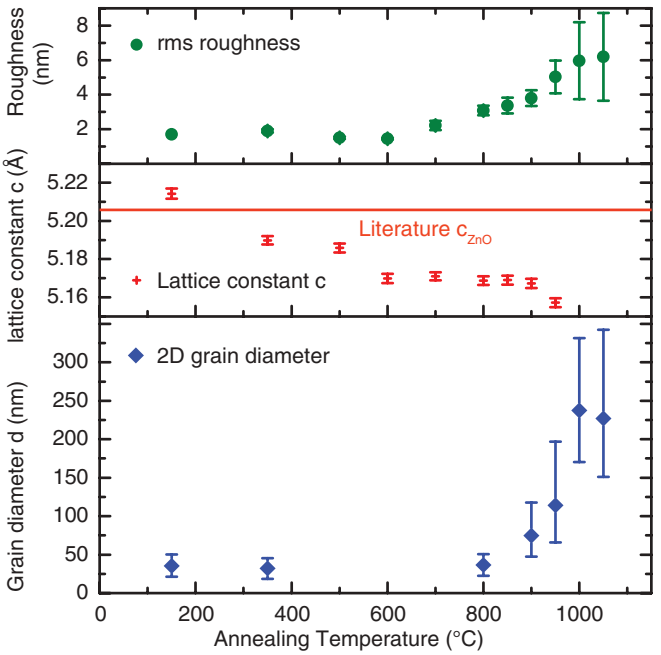

FIG. 2. (Color online) Grain diameter [(blue) diamonds], ZnO lattice constant c [(red) crosses], and rms roughness [(green) circles] in dependence of the annealing temperature.

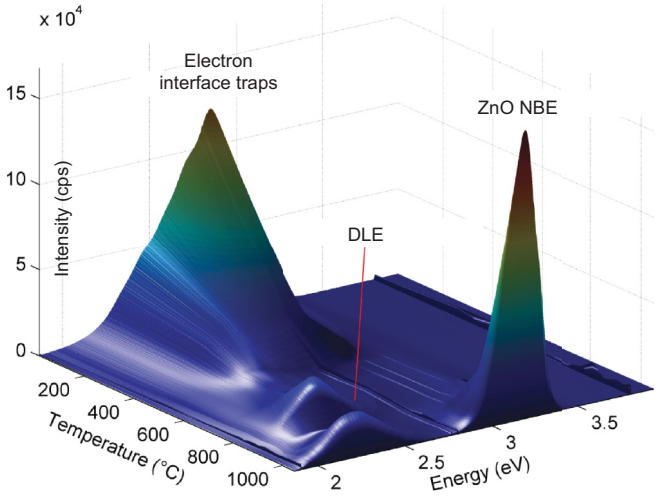

FIG. 3. (Color) Photoluminescence intensity as a function of photon energy and annealing temperature.

ambiguous, this value is probably a little bit too large. AFM measurements additionally show that the rms roughness as a function of the annealing temperature [Fig. 2; (green) circles] increases as expected with the increasing grain diameter. Furthermore, we determined the c-lattice constants of the ZnO film from the x-ray data as a function of the annealing temperature [Fig. 2; (red) crosses]. The overall strain is very low, as the resulting lattice constants are very close to the bulk literature value. With increasing annealing temperature, the lattice constant c decreases, probably due to the presence of the Si(111) surface, which has a larger in-plane lattice constant than bulk wurtzite ZnO.

We obtain information on the electronic properties of the film from PL measurements. Figure 3 shows the room-temperature PL after each separate annealing step. The PL of the as-grown sample is shown at a growth temperature of $T = 150\,^{\circ}$C. Two different regimes can be distinguished: The low-temperature regime ($T \leqslant 600\,^{\circ}$C), which is dominated by a broad blue emission band at ∼2.85 eV; and the high-temperature regime ($T > 600\,^{\circ}$C). The broad peak at 2.85 eV in the low-temperature regime cannot be attributed either to the near-band-edge (NBE) recombination or to the well-known yellow-green deep-level emission (DLE) at ∼2.3 eV, which is present in many ZnO samples and is typically attributed to intrinsic point defects, such as oxygen vacancies V_O[17] or Zn vacancies V_{Zn}.[18] Other intrinsic defects in ZnO that could be responsible for the recombination band at 2.85 eV are the interstitials Zn_i and O_i as well as the antisite defects Zn_O and O_{Zn}. Recent density functional calculations using an extrapolated LDA + U approach[19] or the GW method[20] find no intrinsic defect in ZnO which is likely to have transition energies that match the observed recombination band. Moreover, the energy difference between the recombination band and the ZnO bulk NBE recombination is too large to be caused by strain. Thus, we associate the blue emission with electron interface traps located at the ZnO-ZnO grain boundaries as suggested by Cordaro *et al.*[21] The stepwise annealing in an oxygen atmosphere leads to a significant change in the PL signal. Up to 600 °C, we observe a clear energy red-shift to 2.3 eV and a substantial intensity decrease. This can be explained by a grain boundary diffusion-driven crystallization.[22] In the high-temperature regime, above 600 °C, NBE recombination develops and a less intense luminescence band at 2.3 eV from intrinsic defects appears.

The missing of significant NBE recombination in the low-temperature regime strongly suggests the presence of small grains in the film. This granular structure is caused by the short surface diffusion length at 150 °C and the large lattice mismatch between ZnO and Si. The ZnO-ZnO grain boundary represents a double Schottky barrier with a depletion region on both sides. Within this region the electron-hole pairs are recombining mainly via the deep donor levels. Therefore for smaller particles, the width of the depletion region is the limiting factor for the NBE PL. Assuming a spherical shape and depletion layer widths of around 15–30 nm,[23,24] for grains with diameters $\leqslant$50 nm, only a weak NBE signal is expected.

HRXRD reciprocal space maps were recorded to determine the entire structural information including the crystal orientation, structure, and quality of the as-grown sample and the sample annealed at the highest temperature. In Fig. 4 the XRD intensity is plotted as a color scheme in the reciprocal space as a function of the wave numbers $q_\perp$ and $q_\parallel$. The wide spot at a $q_\perp$ value of 2.37 Å^{-1} belongs to the (0002) reflex of the grown ZnO layer; the smaller spot, at a $q_\perp$ value of 1.96 Å^{-1}, to the (111) reflex of the silicon substrate. The broad curved shape of the ZnO reflex in the as-grown map reveals a strong mosaic character. After annealing at 1050° C the mosaicity is clearly reduced due to the coalescence of the grains. As expected, the ZnO c direction is preferably oriented parallel to the Si(111) direction as observed by a complete range $\omega/2\theta$ scan.

Additionally, we performed ω scans to obtain information on the crystal quality, mainly on the mosaicity and defect density. These rocking curves of the ZnO(0002) reflex were also recorded after each annealing step and are shown in Fig. 5. In the low-temperature regime, the films exhibit a strong mosaic character. Up to an annealing temperature of 600 °C we observe just a slight decrease in the FWHM. In this regime the annealing mainly affects the intrinsic point defects, while the grain size of the ZnO clusters remains almost the same as confirmed by AFM measurements. In the high-temperature regime, annealing temperatures above 600 °C cause extensive changes in the ZnO film. A strong decrease in the FWHM confirms a substantial improvement of the crystal quality above 600 °C. At higher temperatures the FWHM of the ZnO(0002) rocking curve still decreases and saturates at about 1.1°. At temperatures up to 1050 °C, a narrowing by a factor of 3 compared to the as-grown film is achieved (see inset in Fig. 5). Three properties contribute to the rocking curve FWHM: the density of dislocations, the presence of small grains, and the mosaicity. Here, the dominant contribution is the mosaicity, as lots of small, slightly tilted regions not only scatter according to their particular orientation but also promote the formation of small-angle grain boundaries. The considerable narrowing of the rocking curve by thermal treatment therefore indicates a reorientation of the ZnO grains following the (111) direction of the silicon substrate. The formation of this preferred

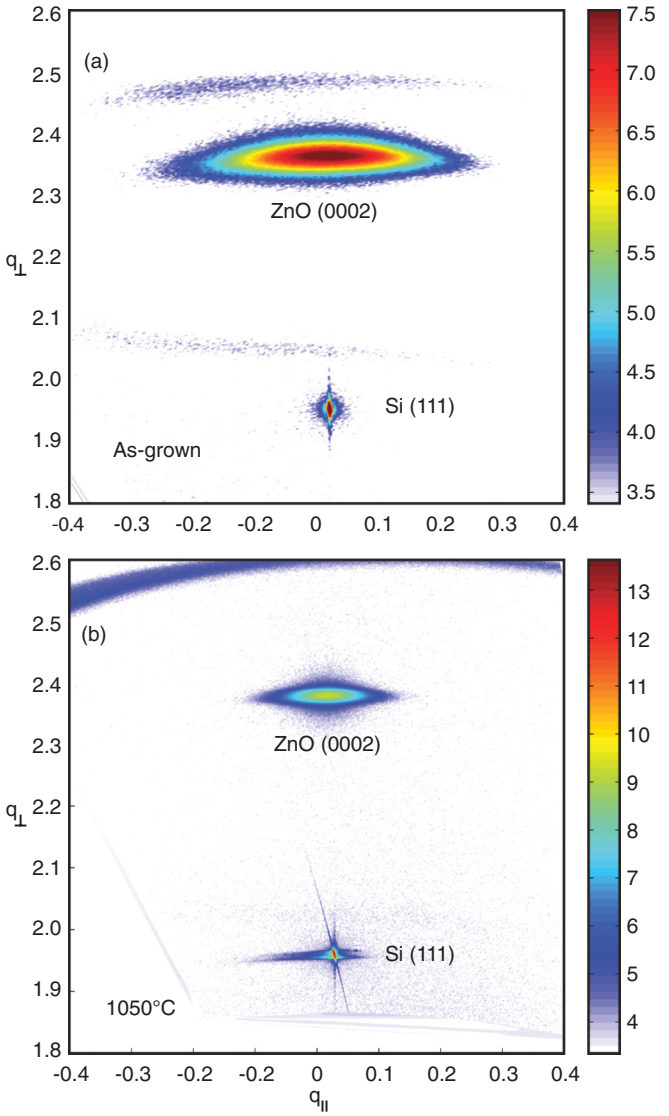

FIG. 4. (Color online) (a) XRD intensity plotted as a reciprocal space map of the as-grown sample compared with (b) that after the annealing step at 1050 °C.

orientation is caused by the realignment of tilted grains by rotation and merging with the dominating (0002) grains. As a consequence, the spot in the reciprocal space map as well as the rocking curve peak becomes narrow. Using AFM the grain sizes are determined. The results confirm the above conclusions.

We investigate the orientation of individual grains in detail by EBSD measurements. In this way, not only the grain boundaries, but also their orientation and the alignment of the grains towards each other can be analyzed. As in three-dimensional (3D) crystals not only an in-plane twist rotation, but also a tilt rotation perpendicular to the substrate surface is possible, two degrees of freedom have to be taken into account. In Fig. 6 the corresponding pole figures of the annealed sample (1050 °C, O_2 atmosphere) are shown in the insets and weighted by the size of the grains. While almost all grains are oriented along the *c* axis in the (0001) direction after the thermal treatment, the in-plane rotation angles are more widely

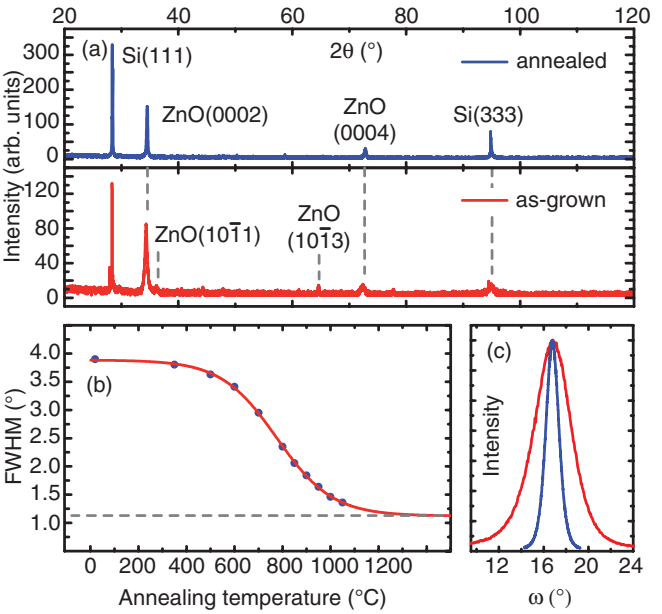

FIG. 5. (Color online) (a) HRXRD $\omega/2\theta$ scans of the as-grown sample [bottom (red)] and the annealed [top (blue)] sample. (b) The FWHM of the ZnO (0002) rocking curve decreases with increasing annealing temperature. (c) Corresponding normalized rocking curves of the ZnO (0002) peak: initially [outer (red) curve] and thermally treated at 1050 °C [inner (blue) curve].

distributed [see the pole figure for the {10$\bar{1}$0} orientation]. The in-plane hexagonal ordering is clear proof that the ZnO grains are no longer randomly oriented but follow the symmetry of the Si(111) surface. Smaller grains are still twisted, as they require longer time scales to coalesce with the reoriented, larger

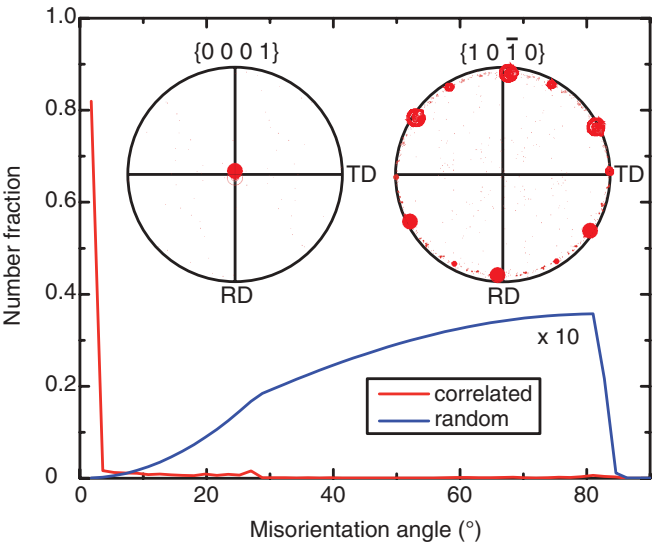

FIG. 6. (Color online) Distribution of the misorientation angle of the annealed (red) and a random oriented (blue) sample. Insets: Pole figures of the ZnO layer surface after 1 h of annealing at 1050 °C, weighted by grain size for the {0001} orientation and the {10$\bar{1}$0} orientation. In both cases, the normal direction is parallel to the Si(111) direction, while the rolling direction (RD) and transverse direction (TD) are in-plane.

grains. The disorientation angle distribution shown in Fig. 6 shows that, after annealing, the system is highly correlated, dominated by low-angle grain boundaries. This distribution is clearly different from the Mackenzie distribution[25] for random polycrystalline samples, which is also shown for comparison.

In the next step, we determine the dynamics of the coalescence and growth from the experimental results. Here, we need to know how the volume of grains relates to a microscopic time scale. Therefore, from a careful analysis of the AFM measurements after each annealing step, the mean grain size is determined from log-normal fits of the histograms. For three different annealing temperatures AFM images as well as histograms obtained from the AFM measurements are shown in Fig. 1. The others are given in the Supplemental Material.[16] The mean grain diameters vary between 35 and ~250 nm.

The diffusion length is estimated from the increase in the mean grain diameter ($L_D = d - d_0$). The macroscopic process time t_{proc} (annealing time), the temperature T, the diffusion length, and the activation energy E_A are related via Einstein's relation,

$$L_D = \sqrt{D(T) \cdot t_{proc}}, \tag{1}$$

where $D(T)$ is the solid-state diffusion coefficient,

$$D(T) = D_0 \exp\left(-\frac{E_A}{k_B T}\right). \tag{2}$$

As L_D, t_{proc}, and T are known from the experiment, the diffusion coefficient $D_0 = (0 \pm 2) \times 10^{16}$ nm^2/s and the activation energy $E_A = (3.8 \pm 0.6)$ eV can be obtained from an Arrhenius plot (note that the error for D_0 is quite large due to the strong sensitivity of this quantity to E_A). Under the assumption of a constant rate of diffusive grain growth $v_D = L_D/t_{proc}$, the macroscopic quantities L_D and t_{proc} can be related to the corresponding microscopic quantities, i.e., the lattice constants a and c as well as the kinetic time scale $\tau_{a,c}$, which is the mean time for an atomic site diffusion process:

$$v_D := \frac{L_D}{t_{proc}} = \frac{a,c}{\tau_{a,c}}. \tag{3}$$

The corresponding average grain volumes V in the spherical approximation are normalized to the initial value V_0 and shown in a double-logarithmical plot against the kinetic time scale $\tau_{a,c}$ (Fig. 7). As at low temperatures the reorganization process will be very slow, it will be extremely fast at very high temperatures. Therefore $T = 900^\circ$ C was used as the reference temperature, which is in the middle of the temperature range of the grain growth process. At any rate, the reference temperature has no influence on the slope of the function, which appears to have a linear behavior in the logarithmic plot. Considering that at the last two points a saturation regime might be reached, the fitting has to be done on the first four points and the linear behavior is not as clear. This assumption could be corroborated by the thickness of the initial ZnO layer of around 200 nm. But as the mean diameters of both points are already larger than 200 nm and clearly higher values are also observed, and the number of grains analyzed at 1000 °C is very low, we treat this value as not being very accurate.

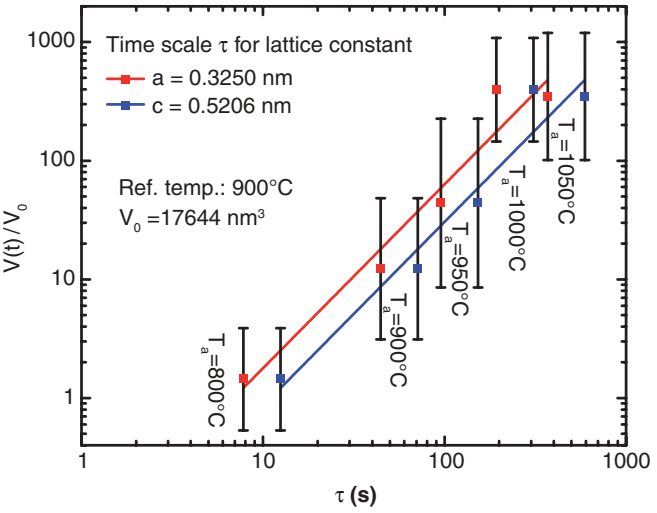

FIG. 7. (Color online) Time dependence of the average grain volume normalized to the initial value at a reference process temperature of 900 °C for lattice constants $a = 0.325$ nm [left (red) line] and $c = 0.5206$ nm [right (blue) line] of ZnO.

As the linear fit of the data lies within its error bar, we believe that it is justified. The experimental data are consistent with a 3D growth exponent as large as $n = 1.55$ for the in-plane lattice constant a as well as for the out-of-plane lattice constant c. From this, we obtain the grain-rotation mobility parameter,[13]

$$p = \frac{2}{n} + 1 \approx \frac{7}{3}. \tag{4}$$

It should be noted that a smaller mobility parameter corresponds to faster coalescence and growth. Comparing our result for p with the calculations performed by Moldovan *et al.*[13] in two dimensions, the grain-rotation mobility parameter p in our 3D system is significantly lower than in two dimensions. The faster coalescence and growth in 3D can be explained by the additional degree of freedom, the tilt rotation, which is not present in two dimensions. Although the as-grown film already has a significant preference along the Si(111) orientation, the annealing and the substrate influence strongly promote tilt processes towards this direction. This can also be seen from the XRD $\omega/2\theta$ scans [Fig. 5(a)] as well as from the EBSD {0001} pole figures (Fig. 6). Thus we conclude that such tilt processes occur frequently enough to have a significant impact on the growth scaling coefficient.

In summary, we have demonstrated the three-dimensional grain-rotation-induced coalescence of grains in a polycrystalline ZnO film on a Si(111) substrate by thermal annealing. Based on Einstein's law of diffusion a kinetic time scale has been calculated. The grain growth follows the power law $V(t) \sim \tau^n$ with a growth exponent of ~1.5. Thus recrystallization is much faster than in two dimensions due to the increased degrees of freedom in three dimensions.

Professor D. Wolf is acknowledged for helpful discussions. We thank Professor G. Eggeler and N. Lindner for performance of the EBSD measurements and the BMBF for support via NanoFutur Grant No. 03X5509.

[1]H. J. Ko, Y. F. Chen, S. K. Hong, H. Wenisch, T. Yao, and D. C. Look, Appl. Phys. Lett. **77**, 3761 (2000).
[2]S. Sadofev, S. Blumstengel, J. Cui, J. Puls, S. Rogaschewski, P. Schafer, Y. G. Sadofyev, and F. Henneberger, Appl. Phys. Lett. **87**, 091903 (2005).
[3]M. Kubo, Y. Oumi, H. Takaba, A. Chatterjee, A. Miyamoto, M. Kawasaki, M. Yoshimoto, and H. Koinuma, Phys. Rev. B **61**, 16187 (2000).
[4]M. R. Wagner, T. P. Bartel, R. Kirste, A. Hoffmann, J. Sann, S. Lautenschläger, B. K. Meyer, and C. Kisielowski, Phys. Rev. B **79**, 035307 (2009).
[5]J. J. Zhu, B. X. Lin, X. K. Sun, R. Yao, C. S. Shi, and Z. X. Fu, Thin Solid Films **478**, 218 (2005).
[6]M. Fujita, N. Kawamoto, M. Sasajima, and Y. Horikoshi, J. Vac. Sci. Technol. B **22**, 1484 (2004).
[7]R. Theissmann, M. Fendrich, R. Zinetullin, G. Guenther, G. Schierning, and D. E. Wolf, Phys. Rev. B **78**, 205413 (2008).
[8]A. Sánchez, A. R. Bishop, D. Cai, and N. Grønbech-Jensen, Phys. Rev. B **52**, 5433 (1995).
[9]A. J. Detor, Phys. Rev. B **78**, 144113 (2008).
[10]C. G. Granqvist and R. A. Buhrman, Appl. Phys. Lett. **27**, 693 (1975).
[11]C. D. Pownall and P. A. Mulheran, Phys. Rev. B **60**, 9037 (1999).
[12]J. E. Rubio, M. Jaraiz, I. Martin-Bragado, J. M. Hernandez-Mangas, and G. H. Gilmer, J. Appl. Phys. **94**, 163 (2003).
[13]D. Moldovan, V. Yamakov, D. Wolf, and S. R. Phillpot, Phys. Rev. Lett. **89**, 206101 (2002).
[14]L. J. Moore, R. D. Dear, M. D. Summers, R. P. A. Dullens, and G. A. D. Ritchie, Nano Lett. **10**, 4266 (2010).
[15]A. Redondo-Cubero, M. Vinnichenko, M. Krause, A. Mücklich, E. Muñoz, A. Kolitsch, and R. Gago, J. Appl. Phys. **110**, 113516 (2011).
[16]See Supplemental Material at http://link.aps.org/supplemental/10.1103/PhysRevB.86.224108 for more details on the AFM, XRD, and EBSD measurements, the annealing procedure, and other information.
[17]F. H. Leiter, H. R. Alves, A. Hofstaetter, D. M. Hofmann, and B. K. Meyer, Phys. Status Solidi B **226**, R4 (2001).
[18]A. F. Kohan, G. Ceder, D. Morgan, and Chris G. Van de Walle, Phys. Rev. B **61**, 15019 (2000).
[19]A. Janotti and C. G. Van de Walle, Phys. Rev. B **76**, 165202 (2007).
[20]R. Ramprasad, H. Zhu, P. Rinke, and M. Scheffler, Phys. Rev. Lett. **108**, 066404 (2012).
[21]J. F. Cordaro, Y. Shim, and J. E. May, J. Appl. Phys. **60**, 4186 (1986).
[22]D. Moldovan, D. Wolf, and S. R. Phillpot, Acta Mater. **49**, 3521 (2001).
[23]W. G. Morris, J. Vac. Sci. Technol. **13**, 926 (1976).
[24]T. R. N. Kutty and S. Ezhilvalan, J. Phys. D **29**, 809 (1996).
[25]J. K. Mackenzie, Biometrika **45**, 229 (1958).